20th Australasian Fluid Mechanics Conference
Perth, Australia
5-8 December 2016

Streak Linear Stability and its Sensitivity to Free-stream Vortical Forcing

D. A. Pook and J. H. Watmuff

School of Engineering
RMIT University, Victoria 3083, Australia

Abstract

Computations of steady streak linear stability in an adverse pressure gradient near a leading edge are presented. Streaks forced by free-stream normal or streamwise vorticity show different linear stability characteristics near the leading edge. With sufficient streamwise distance, the characteristics are similar. The results have implications for interpreting bypass transition.

Introduction

The simulations of Nagarajan et al. [6] involving FST interacting with the leading edge revealed multiple transition scenarios. Increasing free-stream turbulence levels and a blunter leading edge changed the transition process from sinuous streak secondary instability, to wave-packet growth in high-speed streak regions. The wave-packets were traced back to normal vorticity wrapping around the leading edge. Tollmien-Schlichting waves (TS) were ruled out of the transition scenario due to the high frequencies and phase speeds. Goldstein and Sescu [4] have shown that unsteady streaks in a Blasius layer, created by normal vorticity, can remain inflectional in the high-speed region and support inviscid wave-packet growth. Goldstein [1] has suggested there are two classes of streaks which are generated from the free-stream: streamwise vorticity streaks (ω_x) [2, 9] that are insensitive to the leading edge; normal vorticity streaks (ω_y) [3] that are sensitive to the leading edge.

Here, the simpler case of steady streaks forced from either streamwise or normal vorticity, and their influence on TS linear stability studied. Streak secondary instability is not considered.

Geometry and Computational Methods

Laminar Base-flow

Streak base-flows are calculated with ANSYS Fluent. The steady, pressure-based, coupled solver is used with 3rd order MUSCL for momentum terms and PRESTO for pressure. Pook [7] verifies accuracy using a Blasius boundary layer.

Two-dimensional Base-Flow

The Base-flow models a wind-tunnel consisting of a two-dimensional, 5:1 contraction and a flat plate mounted away from the tunnel centreline. This is the same configuration described by [8], except for a blunt leading edge defined by,

$$(x/a)^6 + (y/h)^2 = 1, \tag{1}$$

where a is the leading edge length and h is the half-width. The aspect ratio (a/h) is 9, spanwise (z) width is $0.583a$, and Reynolds number based on a is 22,200. A wind tunnel configuration is used to capture potential issues that would affect experimental reproduction of results. Approximately 110 cells are used through the boundary layer, 1000 cells in the streamwise direction to $x = 5a$, and 120 cells across the span. The total test-section mesh size is approximately 60 million.

Flow attachment on the leading edge centreline produces an adverse pressure gradient (see figure $1a$) until $x \approx 13a$. This is due to a small mismatch of roof geometry and layer growth. The maximum shape factor of $H = 2.98$, is comparable to [6]. Figure $1(c)$, the neutral stability calculated with Orr-Sommerfeld equations, indicates TS growth near the leading edge. The boundary layer is unstable to extremely high frequencies,

$$F = \omega\nu U^{-2} \times 10^6, \tag{2}$$

where ω is the circular frequency, ν is the kinematic viscosity, and U is the free-stream velocity. Forcing attachment on the leading edge topside (slot mass-flow of 0.21, see [8]) removes the pressure gradient and the neutral stability is close to that of a Blasius layer. Centreline attachment is used in this paper.

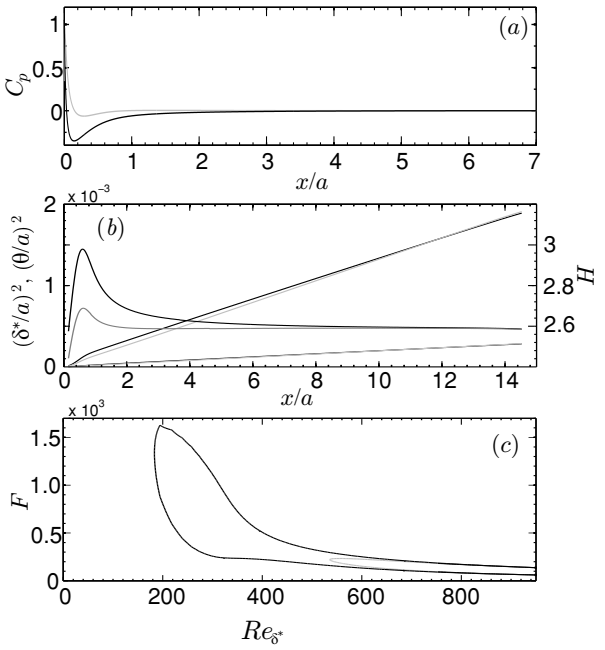

Figure 1: Two-dimensional base-flow. Black: centreline attachment. Grey: topside attachment. (a) Pressure coefficient (C_p) (b) Displacement thickness (δ^*), momentum thickness (θ), and shape-factor (H). (c) Neutral stability envelope.

Steady Streak Boundary Conditions

A sinusoidal spanwise disturbance of the free-stream velocity is used to create the streaks. The disturbance is defined by,

$$\Delta U = -A_f \times U \cos\left(\frac{2\pi}{0.583a} z\right), \tag{3}$$

where A_f sets the disturbance amplitude. Normal vorticity streaks are created by introducing the disturbance at the inlet of the test-section mesh, $4.8a$ upstream of the leading edge. For streamwise vorticity streaks, the disturbance is introduced upstream of the contraction, $62.5a$ upstream of the leading edge. Passage of the disturbance through the contraction creates streamwise vorticity [8]. Table 1 lists the disturbance amplitudes used.

Normal Vorticity		Streamwise Vorticity	
Name	A_f	Name	A_f
N2	0.02	S5	0.05
N5	0.05	S10	0.10
N10	0.10	S20	0.20
N15	0.15	S30	0.30

Table 1: Parameters of the sinusoidal free-stream disturbance.

Figure 2 shows the wake vorticity on a line $1.84a$ upstream of the leading edge, and the resultant streak amplitude. The streak amplitude is defined by,

$$A(x) = \left(\max_{y,z}(U-U_{2d}) - \min_{y,z}(U-U_{2d})\right)/2U_e, \quad (4)$$

where U_{2d} is the two-dimensional base-flow velocity profile. The highest amplitude disturbances show distortion. Streamwise vorticity creates stronger streaks, even with the blunt leading edge.

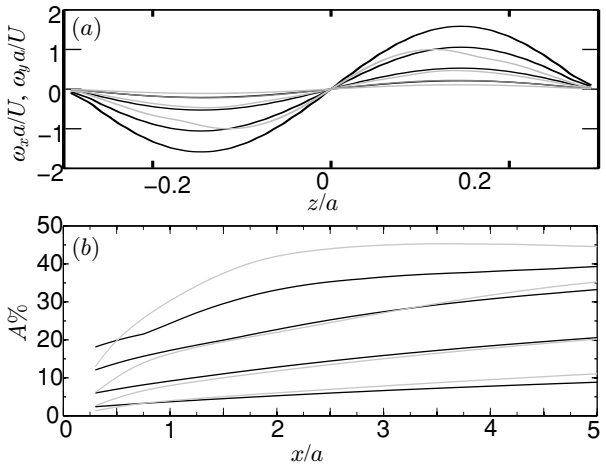

Figure 2: (a) Wake $1.84a$ upstream of the leading edge. (b) Streak amplitude. Black: normal vorticity. Grey: streamwise vorticity.

BiGlobal Linear Stability

Streak linear stability is computed with BiGlobal stability equations using Fourier decomposition in the spanwise direction. The base-flow, $\mathbf{U} = (U,V,W)^{\mathrm{T}}$, is decomposed as,

$$\mathbf{U} = \sum_{k=-N}^{N} \hat{\mathbf{U}} \exp(ik\beta z) \quad (5)$$

where β is the spanwise wavenumber. Assuming parallel flow in the streamwise direction (x) allows the definition of a disturbance, $\mathbf{q}(x,y,z,t) = (u,v,w,p)^{\mathrm{T}}$ as,

$$\mathbf{q} = \sum_{k=-N}^{N} \hat{\mathbf{q}} \exp(i\alpha x + i(k+\varepsilon)\beta z - i\omega t), \quad (6)$$

where α is the complex streamwise wavenumber, ω is the real angular frequency, and ε is the Floquet parameter. The spatial eigenvalue problem is formulated for a given wavenumber (k) as,

$$\sum_{j=-\infty}^{+\infty} L_1^{k-j}\hat{\mathbf{q}}^j + L_2^{k-j}\hat{\mathbf{q}}_y^j + C^{k-j}\hat{\mathbf{q}}_{yy}^j = -i\alpha D^{k-j}\hat{\mathbf{q}}^j + \alpha^2 C^{k-j}\hat{\mathbf{q}}^j, \quad (7)$$

where subscript y is the wall-normal derivative. The matrices L_1, L_2, C and D can be found in [7]. Only the U and W component of the base-flow are used. The polynomial eigenvalue problem is made linear with the substitution used by [5] for the OS equation. Equation (7) is solved with the Arnoldi method via the Matlab eigs function calling ARPACK. The wall-normal (y) direction is differenced with Chebyshev polynomials on N_p Chebyshev–Gauss–Lobatto collocation points, mapped algebraically to the physical domain $[0 \ldots y_{max}]$ with half the points placed below y_c. The boundary conditions are,

$$y(0) : u,v,w = 0, \quad y(y_{max}) : u,v,w = 0. \quad (8)$$

The base-flow is linearly interpolated onto the BiGlobal grid. Assessment of grid resolution is shown in Table 2 using the N10 streak at $x = 2a$, computing the most unstable eigenvalue for $\omega = 1750$ rads^{-1} and $\varepsilon = 0$. Using $N_p = 80$, $k = [-20 \ldots 20]$, $y_c = 2\delta_{99}$, and $y_{max} = 10\delta_{99}$ (δ_{99} is the two-dimensional layer 99% thickness) changes the eigenvalue by 0.11% relative to a solution with N_p and y_{max} doubled. Increasing k beyond 20 has no substantial effect, and the resolution $N_p = 80$, $y_c = 2\delta_{99}$, $y_{max} = 10\delta_{99}$, $k = 20$, is used in subsequent calculations. Base-flow resolution is assessed by halving the Fluent CV in each direction. Table 2 shows the eigenvalue changes by 1.2%. The full base-flow mesh resolution is used for all calculations and is considered accurate enough to determine qualitative behaviour.

N_p	y_c (δ_{99})	y_{max} (δ_{99})	k	$\alpha_r\delta^*$ $\times 10^{-1}$	$-\alpha_i\delta^*$ $\times 10^{-3}$	$\Delta\lvert\alpha\rvert$ %
‡160	4	20	20	2.801	2.453	0.00
80	2	5	20	2.800	2.430	0.97
80	2	10	5	2.795	1.955	20.3
80	2	10	15	2.801	2.456	-0.13
†80	2	10	20	2.801	2.456	-0.11
80	2	10	25	2.801	2.456	-0.11
*80	2	10	20	2.801	2.424	1.20

Table 2: Resolution affect on eigenvalue accuracy. † resolution used in subsequent calculations. ‡ reference eigenvalue for $\Delta|\alpha|\%$. $*$ calculated from halving Fluent base-flow CV.

Linear Stability Results

On the Leading Edge ($x = 0.5a$)

Streak base-flows contours at $x = 0.5a$, scaled by the local edge velocity of two-dimensional layer (U_e), are shown in figure 3. The cross-flow velocity of the normal vorticity streaks is reversed near the wall across the entire streak span. Only the S20 and S30 streamwise vorticity streaks exhibit a limited region of reversed cross-flow near the streak centreline.

The eigenvalue spectrum for even and odd modes ($\varepsilon = 0$) are shown in figure 4, and the envelope of the most unstable modes in figure 5(a). Each frequency has a discrete branch of eigenvalues, similar to a two-dimensional layer with disturbances of differing spanwise numbers, i.e. oblique waves. Even and odd eigenvalues have similar values for smaller streak amplitudes, with the most unstable mode even except for S30.

Increasing streak amplitude for normal vorticity streaks suppress low frequencies, except N2 and N5 which slightly destabilise higher frequencies. The most unstable frequency shifts from $F = 1100$ for two-dimensional flow, to $F \approxeq 1400$ for N15, but the growth rate is reduced. The phase velocity defined as,

$$c_r = \omega\alpha_r^{-1}, \quad (9)$$

of the most unstable mode is also increased relative to the two-dimensional TS, up to $0.55U_e$ (see figure 5(b)).

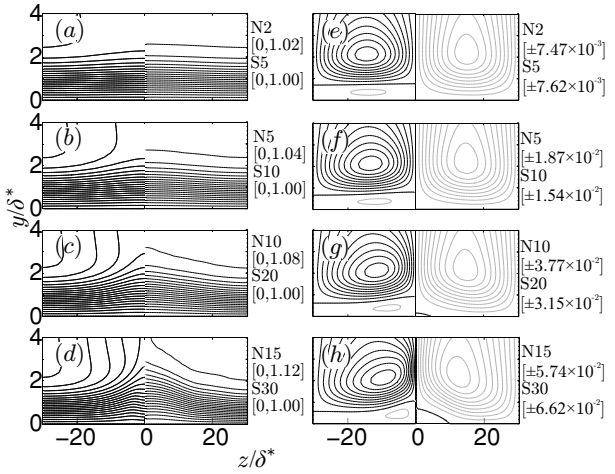

Figure 3: Base-flow contours (20 levels, grey is negative) at $x = 0.5a$, $Re_{\delta^*} = 240$. $z < 0$ is left-side of normal vorticity streak. $z > 0$ is right-side of streamwise vorticity streak. Bracketed values are min/max. U/U_e: (*a*) N2, S5 (*b*) N5, S10 (*c*) N10, S20 (*d*) N15, S30. W/U_e: (*e*) N2, S5 (*f*) N5, S10 (*g*) N10, S20 (*h*) N15, S30.

Streamwise vorticity streaks destabilise lower frequencies ($F < 1200$) with increasing amplitudes. The maximum growth rates exceed that of two-dimensional TS. For S30, the most unstable frequency is $F \approxeq 800$. However, the phase velocity is barely altered. No streak secondary instability modes, based on an expected $c \approxeq 0.8U_e$, are found.

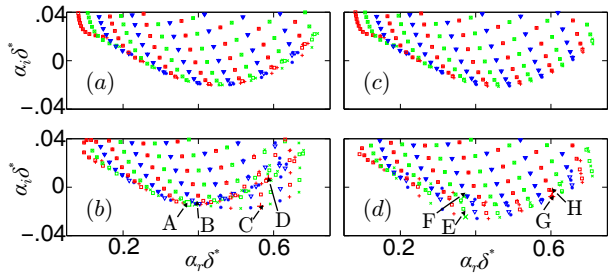

Figure 4: Eigenvalues at $x = 0.5a$. Even modes: $+, \times, *$. Odd modes: $\square, \triangledown$. Colours group the same frequency from F =245 to 1800 (19 frequencies). (*a*) N2 (*b*) N10 (*c*) S2 (*d*) S20.

Figure 6 shows sample eigenvectors for modes labelled A to H in figure 4. For lower frequencies, the most unstable even and odd modes of the normal vorticity streaks (A and B) have their u_{rms} concentrated near the low-speed region of the streak. The modes C, D are even with the same frequency. The mode C u_{rms} is concentrated near the high-speed region of the streak. The w_{rms} maximum is larger than u_{rms}, located further away from the low-speed streak region, and lower in the layer. Characteristics in common with the wave-packets of [6].

Modes E and F, G and H for the streamwise vorticity streaks have the same disturbance frequency. Mode E is characteristic of modes promoted at low frequencies, with u_{rms} concentrated in the low-speed streak region, while F with u_{rms} in the high-speed region is suppressed. At high frequencies, the maximum u_{rms} moves towards the high-speed region (see G) but the growth is slightly reduced relative to two-dimensional TS.

The spanwise periodic streak base-flows are decomposed with a Fast Fourier Transform (FFT) to explore a simplified model of streak stability. Figure 7(*a*) shows the two-dimensional base-

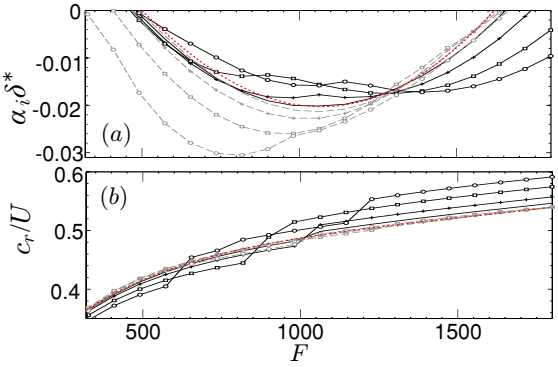

Figure 5: (*a*) Unstable eigenvalue envelope at $x = 0.5a$. (*b*) Phase velocity of the most unstable eigenvalue. Dotted red line is two-dimensional layer. Solid black: N2 no mark; N5 +; N10 □; N15 ○. Dashed grey; S5 no mark; S10 +; S20 ○; S30 □.

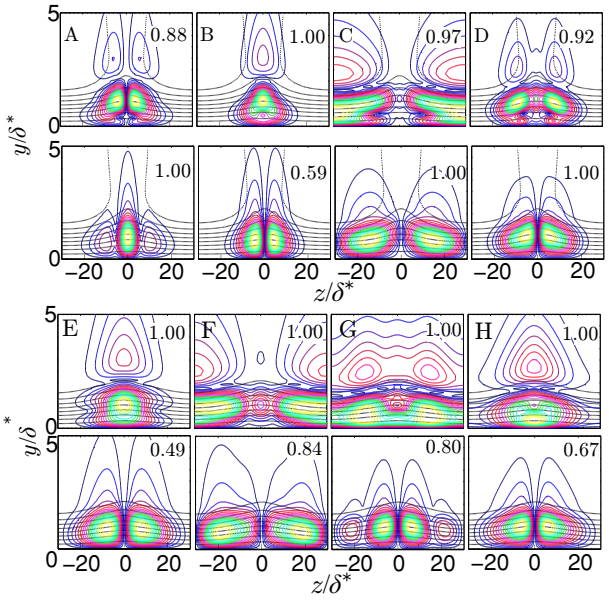

Figure 6: Eigenvectors for eigenvalues, A–H, in figure 4. 20 contour levels, max level in figure. Dotted lines streak base-flow. Top row u_{rms}. Bottom w_{rms}.

flow velocity profile with the inflection point marked. The inflection point could be expected to dominate the stability characteristics. Streaks would alter the stability by shifting the inflection point. Also shown is the zeroth mode deviation ($\hat{U}_d$),

$$\hat{U}_d = \hat{U}^{k0} - U_{2d}, \tag{10}$$

where $\hat{U}^{k0}$ is the zeroth mode (mean) of the base-flow spanwise Fourier decomposition. Figure 7(*b*) shows the $\hat{U}_d$ profile of the streamwise vorticity streaks is "s" shaped. The normal vorticity streak $\hat{U}_d$ show an excess through the entire layer with the maximum above the inflection point.

The streak base-flow modes $\hat{U}^{k\pm1}$, $\hat{U}^{k\pm2}$ are shown in figure 7($c-d$). For all streaks, the maximum of $\hat{U}^{k\pm1}$ is located above inflection point. The $\hat{U}^{k\pm1}$ maximum is located slightly higher for the normal vorticity streaks.

Stability calculations in Figure 8(*a*) using only $\hat{U}^{k0}$, shows this component for the normal vorticity streaks suppresses low-frequency modes and destabilises the higher frequencies. Qualitatively the same as the BiGlobal calculations using all base-flow Fourier modes. Including $\hat{U}^{k\pm1}$, figure 8(*b*), increases the

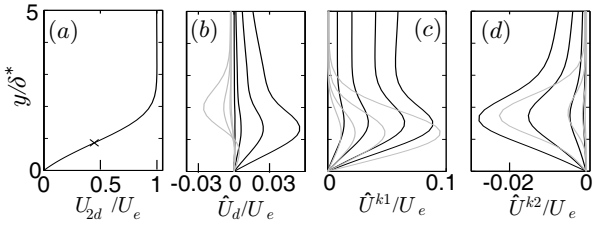

Figure 7: Streak FFT at $x = 0.5a$. (a) U_{2d}, $\times$ inflection point. (b) $\hat{U}_d$, (c) $\hat{U}^{k\pm1}$, (d) $\hat{U}^{k\pm2}$. Black lines normal vorticity streak, grey streamwise vorticity.

growth rate of the high frequencies but the qualitative trend is the same.

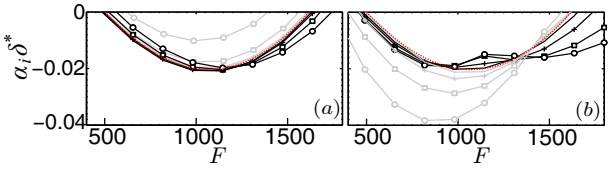

Figure 8: Stability model at $x = 0.5a$: (a) $\hat{U}^{k0}$ only (b) $\hat{U}^{k0}$ and $\hat{U}^{k\pm1}$. Dotted red line is U_{2d} stability. Markers as for figure 5.

Figure 8 shows modification of $\hat{U}^{k0}$ by the streamwise vorticity streaks stabilises all frequencies, unlike the previous BiGlobal calculations. Including $\hat{U}^{k\pm1}$ destabilises low frequencies in qualitative agreement with the BiGlobal calculations.

It can be inferred from figure 7(b) and (c), that the maximum amplitude of $\hat{U}_d$ relative to $\hat{U}^{k\pm1}$ for the normal vorticity streaks increases with streak amplitude, while for the streamwise vorticity streaks it is near constant. Hence, mean flow modification due to the normal vorticity streaks dominates the stability characteristics at this streamwise position while it has a minimal affect for the streamwise vorticity streaks which are dominated by $\hat{U}^{k\pm1}$. The mean flow modification $\hat{U}_d$ is generally stabilising, while $\hat{U}^{k\pm1}$ is destabilising.

Downstream of the Leading Edge ($x = 5a$)

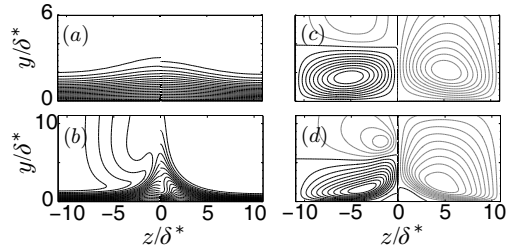

Figure 9: Base-flow contours (20 levels, grey is negative) at $x = 5a$, $Re_{\delta^*} = 616$. $z < 0$ is left-side of normal vorticity streak. $z > 0$ is right-side of streamwise vorticity streak. (a) N2, S5 (b) N15, S30. W/U_e: (c) N2, S5 (d) N15, S30.

Figure 9 shows that, except for the freestream, the streak base flows are visually similar at $x = 5a$. Only the weakest streaks, N2 and S5, still have unstable eigenvalues with TS speeds (see figure 10(a) and (b)). Streak secondary instabilities are present for higher streak amplitudes but not discussed. Inferring from figure 10$(c$-$e)$, the ratio of $\hat{U}_d$ to $\hat{U}^{k\pm1}$ is now similar for both streak types, and the relatively stronger $\hat{U}_d$ is now sufficient to suppress TS disturbances.

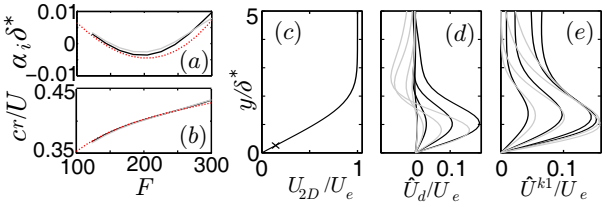

Figure 10: Stability and Base-flow FFT modes at $x = 5a$: (a) Unstable eigenvalue envelope (N2 and S5 only) (b) Eigenvalue phase velocity. (c) $\hat{U}_{2d}$ (d) $\hat{U}_d$ (e) $\hat{U}^{k\pm1}$. Black lines normal vorticity streak, grey streamwise vorticity.

Conclusion

BiGlobal stability calculations have shown free-stream forced, normal and streamwise vorticity streaks have different linear stability characteristics in the early boundary layer. This is attributed to the differing affect on the mean flow, and relative amplitude of the mean flow modification to the first Fourier mode. The unstable high frequency modes of the normal vorticity streaks share similar characteristics with the wave-packets of [6]. Downstream, the qualitative differences diminish.

Acknowledgements

D.A. Pook was funded by the Australian Postgraduate Award (APA). Access to the Trifid HPC cluster and the assistance of the RMIT eResearch Office is gratefully acknowledged.

*

References

[1] M. E. Goldstein, Effect of free-stream turbulence on boundary layer transition, *Philosophical transactions. Series A*, **372**.

[2] M. E. Goldstein and S. J. Leib, Three-Dimensional Boundary-Layer Instability And Separation Induced By Small-Amplitude Streamwise Vorticity In The Upstream Flow, *Journal of Fluid Mechanics*, **246**, (1993), 21–41.

[3] M. E. Goldstein, S. J. Leib and S. J. Cowley, Distortion Of A Flat-Plate Boundary Layer By Free-Stream Vorticity Normal To The Plate, *Journal of Fluid Mechanics*, **237**, (1992), 231–260.

[4] M. E. Goldstein and A. Sescu, Boundary-Layer Transition At High Free-Stream Disturbance Levels- Beyond Klebanoff Modes, *Journal of Fluid Mechanics*, **613**, (2008), 95–124.

[5] H. Haj-Hariri, Transformations Reducing The Order Of The Parameter In Differential Eigenvalue Problems, *Journal of Computational Physics*, **77**, (1988), 472–484.

[6] S. Nagarajan, S. K. Lele and J. H. Ferziger, Leading-Edge Effects In Bypass Transition, *Journal of Fluid Mechanics*, **572**, (2007), 471–504.

[7] D.A. Pook, *The Origin and Effects of Free-Stream Vortical Disturbances on Boundary Layer Transition in Wind Tunnels*, Phd, RMIT University, 2013.

[8] D.A. Pook and J.H. Watmuff, Streak generation in wind tunnels, *Physics of Fluids*, **26**, (2014), 073605.

[9] D. W. Wundrow and M. E. Goldstein, Effect On A Laminar Boundary Layer Of Small-Amplitude Streamwise Vorticity In The Upstream Flow, *Journal of Fluid Mechanics*, **426**, (2001), 229–262.